

# Tunneling Aharonov-Bohm interferometer on helical edge states

R. A. Niyazov,<sup>1,2</sup> D. N. Aristov,<sup>1,3,4</sup> and V. Yu. Kachorovskii<sup>5,2,3</sup>

<sup>1</sup>*NRC “Kurchatov Institute”, Petersburg Nuclear Physics Institute, Gatchina 188300, Russia*

<sup>2</sup>*L. D. Landau Institute for Theoretical Physics, 142432, Moscow Region, Chernogolovka, Russia*

<sup>3</sup>*Institut für Nanotechnologie, Karlsruhe Institute of Technology, 76021 Karlsruhe, Germany*

<sup>4</sup>*St. Petersburg State University, 7/9 Universitetskaya nab., 199034 St. Petersburg, Russia*

<sup>5</sup>*A. F. Ioffe Physico-Technical Institute, 194021 St. Petersburg, Russia*

(Dated: February 21, 2021)

We discuss transport through an interferometer formed by helical edge states tunnel-coupled to metallic leads. We focus on the experimentally relevant case of relatively high temperature as compared to the level spacing and discuss a response of the setup to the external magnetic flux  $\phi$  (measured in units of flux quantum) piercing the area encompassed by the edge states. We demonstrate that tunneling conductance of the interferometer is structureless in ballistic case but shows sharp antiresonances, as a function of magnetic flux  $\phi$  — with the period  $1/2$  — in the presence of magnetic impurity. We interpret the resonance behavior as a coherent enhancement of backward scattering off magnetic impurity at integer and half-integer values of flux, which is accompanied by suppression of the effective scattering at other values of flux. Both enhancement and suppression are due to the interference of processes with multiple returns to magnetic impurity after a number of clockwise and counterclockwise revolutions around setup. This phenomenon is similar to the well-known weak-localization-induced enhancement of backscattering in disordered systems. The quantum correction to the tunneling conductance is shown to be proportional to flux-dependent “ballistic Cooperon”. The obtained results can be used for flux-tunable control of the magnetic disorder in Aharonov-Bohm interferometers built on helical edge states.

PACS numbers:

## I. INTRODUCTION

The quantum interferometry is a rapidly growing area of fundamental research with a huge potential for applications in optics, electronics, and spintronics. One of the simplest realization of quantum electronic interferometer is a ring-geometry setup tunnel-coupled to metallic leads. Such a device can be controlled by magnetic field due to the Aharonov-Bohm (AB) effect [1, 2]. The AB interferometers formed by single or few ballistic quantum channels are very attractive both from a fundamental point of view as prime devices to probe quantum coherent phenomena and in view of possible applications as miniature and very sensitive sensors of magnetic field. Although they have been studied in detail theoretically, their practical implementation faces significant difficulties. The complexity of creating of ballistic single- or few-channel interferometers based on conventional semiconductors, such as GaAs or Si, is connected with technological problems of manufacturing one-dimensional clean systems. The efficiency of quantum electronic interferometers used in practice is limited by rather stringent requirements, for example, very low temperature for interferometers based on superconducting SQUIDS or the requirement of very strong magnetic fields for interferometers based on the edge states of the Quantum Hall Effect systems.

A promising opportunity for a technological breakthrough in this direction is associated with the discovery of topological insulators, which are materials insulating in the bulk, but exhibiting conducting channels at the surface or at the boundaries. In particular, the two-

dimensional topological insulator phase was predicted in HgTe quantum wells [3–5] and confirmed by direct measurements of conductance of the edge states [6] and by the experimental analysis of the non-local transport [7–10]. These states are one-dimensional helical channels where the electron spin projection is connected with its velocity, e.g. electrons traveling in one direction are characterized by spin “up”, while electrons moving in the opposite direction are characterized by spin “down”. Remarkably, the electron transport via helical edge states is ideal, in the sense that electrons do not experience backscattering from conventional non-magnetic impurities, similarly to what occurs in edge states of Quantum Hall Effect systems, but without invoking high magnetic fields (for detailed discussion of properties of helical edge states see Refs. [11, 12]). Hence, in the absence of magnetic disorder, the boundary states are ballistic and the interferometers constructed on such states are topologically protected from external perturbations. Due to this key advantage the helical edge states are very promising candidates for building blocks in quantum spin-sensitive interferometry.

The topological insulators have become a hot topic in the last decade (see Refs. [13–25] and references therein). Particularly, different manifestations of the AB effect in topological insulators were discussed: the dependence of the longitudinal conductance of nanoribbons and nanowires on the magnetic flux piercing their cross-section was studied [16, 24]; weak antilocalization was investigated in the disordered topological insulators and oscillations with magnetic flux with the period equal to the half of the flux quantum were predicted [15, 20].

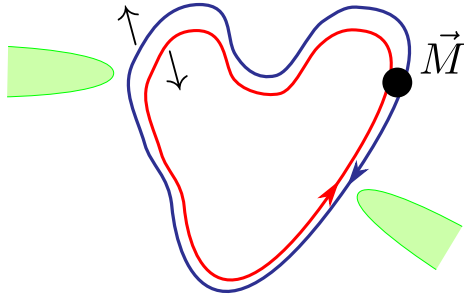


FIG. 1: Interferometer formed by helical edge states tunnel-coupled to the metallic point contacts. The upper shoulder of the interferometer contains magnetic impurity which serves as a backscattering center.

The AB effect was also discussed for almost closed loops formed by curved edge states [18]. Experimentally, the AB oscillations were observed in the magnetotransport measurements of transport (both local and nonlocal) in 2D topological insulators based on HgTe quantum wells [26] and were explained by coupling of helical edges to bulk puddles of charged carriers.

The purpose of the current paper is to discuss a standard AB setup (see Fig. 1) focusing on the effect of the magnetic impurities. We consider an interferometer formed by helical-edge states of a 2D topological insulator tunnel-coupled to leads. We assume that upper and lower shoulders of interferometer have, respectively, lengths  $L_1$  and  $L_2$ . We limit ourselves to discussion of setup with a single impurity placed into upper shoulder at the distance  $s$  (along the edge) from the left contact. This case captures all essential physics of the problem and can be easily generalized for a more general case of arbitrary number of magnetic centers provided that magnetic disorder is weak and the corresponding localization length is large compared to interferometer circumference  $L = L_1 + L_2$ .

Such AB interferometer built on the helical edge states was studied theoretically at zero temperature [13, 19, 23]. It is known, however, that the form and shape of the AB oscillations strongly depend on the relation between temperature  $T$  and level spacing  $\Delta$  connected with the finite size of the system (see a more detailed discussion below). In our case,  $\Delta = 2\pi v_F/L$  is controlled by total length  $L$  and the Fermi velocity  $v_F$ . For typical sample parameters,  $L = 10 \mu\text{m}$ , and  $v_F = 10^7 \text{ cm/s}$ , we estimate the level spacing  $\Delta \approx 3 \text{ K}$ . Having in mind not too low temperatures, we focus on the experimentally relevant case,

$$T \gg \Delta, \quad (1)$$

and discuss dependence of the tunneling conductance  $G$  of the setup on the external magnetic flux  $\Phi$  piercing the area encompassed by edge states. Simple estimates show that the flux quantum,  $\Phi_0 = hc/e$ , is achieved for rings of the above size in fields  $B \sim 3 \text{ Oe}$ , well below the expected magnitude of the fields destroying the edge states

[27–29]. Therefore, in what follows, we neglect the influence of the magnetic fields on the helical states. We will demonstrate the existence of interference-induced effects, which are robust to the temperature, i.e. survive under the condition (1), and can therefore be obtained for relaxed experimental conditions. Specifically, we find that  $G$  is structureless in ballistic case but shows a sharp antiresonances, as a function of  $\phi = \Phi/\Phi_0$  in the presence of magnetic impurities. Although similar antiresonances are known to arise in the single-channel rings made of conventional materials, the helical AB interferometer shows essentially different behavior due to specific properties of the edge states. Most importantly, the effect is more universal and robust to details of the setup, in particular, to the relation between  $L_1$  and  $L_2$ . Another difference concerns the periodicity of the function  $G(\phi)$ , which — for the case of helical edge state interferometer — obeys

$$G(\phi + 1/2) = G(\phi),$$

while for interferometers made of conventional materials, this function is periodic with the period 1.

The resonance behavior of conductance arises due to the interference contribution from trajectories containing multiple returns to the magnetic impurity after ballistic revolutions around the setup in clockwise and counterclockwise directions. Such processes are specific for closed geometry of the system and are absent in the infinite helical edge containing backscattering centers (see discussion of transport in latter system in a number of recent publications [30–36]). We notice, however, that bulk puddles of charged particles coupled to infinite helical edge [31, 32, 35] (or curved edge states with tunneling coupling between different points [18, 30]) can serve as mini-resonators and the edge transport can probe levels in these resonators. This effect was used for interpretation of experimental results on AB oscillations in non-local transport measurements in HgTe quantum well [26]. What we claim here is that for almost closed AB interferometer with very weak tunneling coupling to the leads, the circumference of the interferometer itself can serve as such a resonator and increase or decrease — depending on the value of  $\phi$  — effective scattering on the impurity.

Next, in order to compare our results with previously obtained ones, we briefly summarize the properties of the AB interferometers formed by conventional (non-helical) *single- or few-channel ballistic* channels, which were actively studied in last decades [37–48].

For noninteracting ring, the tunneling conductance of the interferometer,

$$G = N \frac{e^2}{h} \mathcal{T}, \quad (2)$$

is expressed in terms of energy-averaged tunneling transmission coefficient  $\mathcal{T} = -\int d\epsilon \mathcal{T}(\epsilon) \partial_\epsilon f_F(\epsilon)$ , where  $f_F$  is the Fermi distribution function and  $N$  is the number of the conducting channels. The tunneling conductance is

known to exhibit different types of oscillations. Specifically,  $\mathcal{T}(\epsilon)$  oscillates as a function of energy of the tunneling electron  $\epsilon$ , having maxima at positions of quantum levels in the ring [37–39]. For low temperatures,  $T \ll \Delta$ , these oscillations transform into oscillations of  $G$  with the Fermi energy, which are strongly affected by the Coulomb blockade in the interacting case [42]. In the opposite high temperature case,  $T \gg \Delta$ , these oscillations are exponentially suppressed.

Magnetic field applied to the ring leads to AB oscillations —periodic oscillation of  $G$  with the dimensionless magnetic flux  $\phi$  piercing the area encompassed by quantum channels. The period of the oscillations is given by the flux quantum  $\Delta\phi = 1$ . The shape and amplitude of the oscillations depend essentially on the strength of the tunneling coupling and on the relation between  $T$  and  $\Delta$ . For  $T \ll \Delta$  and weak tunneling coupling there are *two narrow resonances* in the dependence  $G(\Phi)$  [37–39] within the interval  $0 < \phi < 1$ . The positions of the resonant peaks depend on the electron Fermi energy [37] and on the strength of the electron-electron interaction [42]. Remarkably, the interference effects are not entirely suppressed with increasing the temperature, and the resonant behavior of  $G(\Phi)$  survives for the case  $T \gg \Delta$ . However, this dependence changes qualitatively. In particular, the high-temperature conductance of the noninteracting ballistic ring with  $L_1 = L_2$  weakly coupled to the contacts exhibits *single sharp antiresonance* in the interval  $0 < \phi < 1$  at  $\phi = 1/2$  [40, 45]. The antiresonances at  $\phi = 1/2 + n$  ( $n$  is integer number) are broadened by weak disorder [46]. The electron-electron interaction leads to appearance of a fine structure of the antiresonances: each antiresonance splits into a series of narrow peaks, whose widths are governed by dephasing [45, 47]. Spin-charge separation in the interacting spinful interferometer leads to the additional splitting of antiresonances because of existence of two types of excitations (charge and spin excitations) propagating with different velocities [40, 48].

Additional physics comes into play in the presence of the spin-orbit (SO) interaction, which results in a phase acquired by the spin part of the electron wave propagating around the ring. This phase is added to AB phase and leads to the third type of the conductance oscillations: periodic oscillations of  $G$  with the strength of the SO coupling, so called Aharonov-Casher (AC) effect [49–51]. The effect of SO on the performance of the AB interferometer was intensively discussed [49–61] with the focus on zero-temperature case. The finite temperature effects were also analyzed both numerically [54, 56, 58], and analytically [62]. In particular, it was found in Ref. [62] that AC effect is also robust to temperature: for  $T \gg \Delta$ , the antiresonances in the conductance are split by SO coupling with the splitting distance proportional to the AC phase.

Since topological insulators are materials where SO interaction is strong, one might expect that the flux dependence of  $G$  in interferometers based on helical edge states

would be very similar to the case of single- or few-channel interferometers based on AC effect. We show below that this is not the case. The antiresonances arising in the usual AB interferometers at high temperatures,  $T \gg \Delta$ , both in absence and in the presence of SO, turn out to be very sensitive to the geometry of the problem [45–48, 62]. In particular, their shape and width are strongly modified for interferometer with non-equal shoulders,  $L_1 \neq L_2$  [70]. By contrast, as we will see, the antiresonances in the interferometers formed by helical edge states are not sensitive to geometry of the device: their amplitude and width do not depend on the relative lengths of the interferometer shoulders and on the position of the magnetic impurity. Also, they do not change in the non-planar geometry of the sample. In the next sections, we present both rigorous calculations and a simple physical interpretation of these properties.

## II. BASIC EQUATIONS

We assume that the helical edge states of two-dimensional topological insulator are tunnel-coupled to metallic nonmagnetic point contacts. We model metallic contacts by single-channel spinful wires, so that electrons are injected into the helical states through so-called tunnel Y junctions. We assume that the electrons in the metallic leads are not polarized. In this paper, we focus on the calculation of the tunneling conductance of the interferometer, whereas interesting effects related to spin-selective properties of the system such as resonance rotation of initial spin polarization will be discussed elsewhere [63].

Since we consider nonmagnetic leads, the different spin projections do not mix at the contacts. Thus, the point contact is described by the time-reversal  $S$ -matrix:

$$S = \begin{pmatrix} -t & r & 0 & 0 \\ r & t & 0 & 0 \\ 0 & 0 & -t & r \\ 0 & 0 & r & t \end{pmatrix}. \quad (3)$$

This  $S$ -matrix connects incoming states  $(l_\uparrow, h_\uparrow, l_\downarrow, h_\downarrow)$  with outgoing states  $(l'_\uparrow, h'_\uparrow, l'_\downarrow, h'_\downarrow)$  (see Fig. 2). “l” stands for the leads, “h” stands for the helical edge. This notation corresponds to one in Ref. [64] after obvious rearrangement of channels. The difference between the Fig. 2a and Fig. 2b is the opposite propagation of electrons with different spins in the helical edge.

The tunneling contact is characterized by two amplitudes  $r$  and  $t$ , obeying  $|t|^2 + |r|^2 = 1$ . Without a loss of generality, we assume that  $t$  and  $r$  are real and express them through the parameter  $\gamma$ ,

$$r = \frac{2\sqrt{\gamma}}{1+\gamma}, \quad t = \frac{1-\gamma}{1+\gamma}, \quad (4)$$

which has a physical meaning of tunneling transparency of the contact [45, 47, 65].

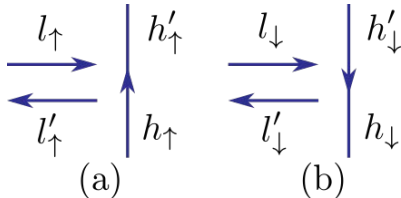


FIG. 2: Point contact between the helical ring and the spinful wire.

Let us calculate the phase acquired by the electron wave after a full revolution around the setup shown in Fig. 1. In order to make the physical picture more transparent, we consider first a general case with two chiralities (direction of propagation) and two spins not necessarily aligned with momentum (this case corresponds to a conventional single-channel spinful wire). The acquired phase includes three terms: a dynamical contribution  $kL$  (here  $k$  is the electron wave vector), magnetic phase  $\pm 2\pi\phi$  and the Berry's phase  $\pm\delta$  [66], given by one half of the solid angle, subtended by spin direction during circumference of the interferometer. The dynamical contribution depends on  $L$  only and does not change its sign when changing the chirality and spin projection. By contrast, the sign of magnetic phase is insensitive to spin but changes sign with changing the chirality. The Berry's phase changes sign both with changing the chirality and with changing the spin (see Tab. I). For helical edge only two electron states are present, which are marked by boldface in the Table I.

Analyzing corresponding phases we arrive at a conclusion, which is of key importance for our analysis. Information about the geometrical structure of the edge states, in particular, about curvature of the edge and/or non-planar geometry, is encoded in the Berry's phase, but as we see, it is simply added to the dynamical phase, which implies that amplitude of any process depends on  $kL + \delta$ . This, in turn, means that tunneling conductance for a given energy (i.e. before thermal averaging) depends on the Berry's phase and is, therefore, sensitive to geometry of the setup. However, for  $T \gg \Delta$ , the thermal averaging implies integration over  $k$  within a wide interval,  $\delta k \sim T/\hbar v_F \gg 1/L$ , around the Fermi wave vector  $k_F$ . After changing integration variable,  $k + \delta/L \rightarrow k'$ , the Berry's phase drops out with the exponential precision. This should be contrasted to the case of conventional interferometers with weak SO coupling, where the Berry's phase contributes to the Aharonov-Casher phase and strongly effects both  $\mathcal{T}(\epsilon)$  and energy-averaged transmission coefficient,  $\mathcal{T}$ . As a result, the conductance of the ring depends on the Berry phase as was first demonstrated in Ref. [52] for low temperature case,  $T \ll \Delta$ , and then generalized for the high temperature regime,  $T \gg \Delta$ , in Ref. [62]. Physically, dependence of  $\mathcal{T}$  on  $\delta$  in the case of weak SO coupling and  $T \gg \Delta$  arises because the electron wave with a given spin polarization can propagate both clockwise and counterclockwise and

		chirality	
		+	-
spin	↑	<b><math>kL + \phi + \delta</math></b>	$kL - \phi - \delta$
	↓	$kL + \phi - \delta$	<b><math>kL - \phi + \delta</math></b>

TABLE I: Phases of electron wave function after a full revolution in the arbitrary setup shown in Fig. 1.

the phase shift between such waves with equal winding numbers,  $n_1 = n_2 = n$ , is given by  $2(\phi + \delta)n$ . Such processes are absent in the interferometer based on helical edge states, and, as a consequence, in the latter case  $\mathcal{T}$  is independent of  $\delta$  in the high temperature regime.

### III. TUNNELING CONDUCTANCE

The tunneling conductance of the setup under discussion is given by Eq. (2) with  $N = 2$ . We have  $G = (2e^2/h)\mathcal{T}$ , where, for the case of spin-unpolarized contacts, the transmission coefficient can be represented as an average over incoming spin polarizations

$$\mathcal{T} = \frac{\mathcal{T}_\uparrow + \mathcal{T}_\downarrow}{2}. \quad (5)$$

For fully ballistic interferometer,  $\mathcal{T}$  does not contain interference term and hence is flux-independent. Indeed, the right- and left- moving electrons have opposite spin projections at any point, in particular at the point contact where they exit the ring. Consequently, they can not interfere in the tunneling process. Next, we take into account that condition (1) provides that  $\delta k L \gg 1$ . Due to this inequality, interference contribution coming from any two trajectories of the same chirality and with different winding numbers  $n$  and  $m$  becomes exponentially small,  $\propto \exp(-\delta k L |n - m|)$ , after the thermal averaging. Neglecting such exponentially small terms, we arrive at the conclusion that only trajectories with the same chirality and  $n = m$  contribute. In other words, the transmission coefficient of fully ballistic system is given by purely classical contributions, while all the interference terms are suppressed. Classical contribution from the trajectory with certain chirality and winding number  $n$  to the transmission coefficient is given by  $|r \cdot t^{2n} \cdot r|^2$ . The summation over  $n$  yields  $\mathcal{T}_\uparrow = \mathcal{T}_\downarrow = r^4/(1 - t^4)$ , and the use of (4) leads to

$$\mathcal{T} = \frac{2\gamma}{1 + \gamma^2}. \quad (6)$$

Here the case  $\gamma \ll 1$  corresponds to weak tunnel coupling mostly considered in this paper, and fully open setup is described by  $\gamma = 1$ .

Let us now demonstrate that the magnetic impurity induces quantum interference corrections to the conductance. We will discuss the case of classical impurity with large magnetic moment  $\mathbf{M}$  ( $M \gg 1$ ). Then, in the first approximation, one can neglect feedback effect related to

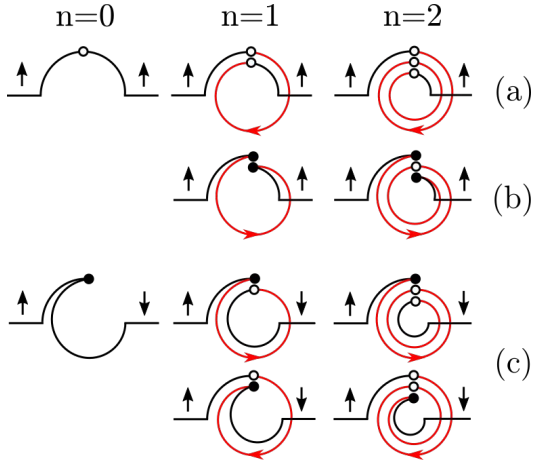


FIG. 3: Processes with incoming spin up projection, involving ballistic propagator as well as single and double backscattering processes at the magnetic impurity. Backscattering events with the corresponding amplitude  $i \sin \theta$  are marked by black dots. Forward scattering events by the magnetic impurity are shown by open circles and has amplitude  $\cos \theta$ . The processes (a) and (b) with coinciding initial and final polarization can interfere. The process (c) corresponds to spin-flip tunneling process. A number of returns to the magnetic impurity denoted by  $n$ . The processes shown in (a) and (b) with equal  $n$  correspond to  $n$  revolutions around the ring in opposite directions.

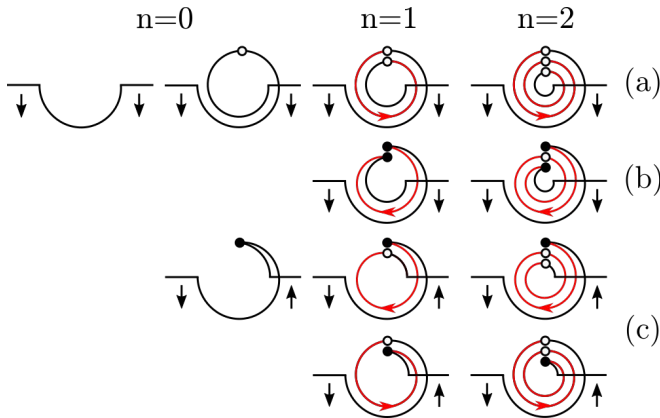


FIG. 4: The same as in Fig. 3 but with spin down projection.

the dynamics of  $\mathbf{M}$  caused by exchange interaction with the ensemble of right- and left-moving electrons (for infinite helical edge this effect was discussed in Ref. [36]).

In this section, we assume that impurity is static and is described by the scattering matrix of general form

$$\hat{S}_M = \begin{pmatrix} \cos \theta & i \sin \theta e^{i\varphi} \\ i \sin \theta e^{-i\varphi} & \cos \theta \end{pmatrix}. \quad (7)$$

with time-independent elements. For such impurity, without a loss of generality, one can put  $\varphi = 0$ . The effects caused by slow random evolution of  $\mathbf{M}$  in the external magnetic bath will be briefly discussed in Sec. V.

The resonant behavior of the conductance appears al-

ready in the perturbative regime, when impurity is weak and  $\theta$  is sufficiently small. Then, one can only keep the corrections to the conductance up to second order with respect to  $\theta$ . Within this approximation one can consider only the ballistic processes and processes with one and two backscattering events. Then, the transmission coefficients for spin  $|\uparrow\rangle$  and  $|\downarrow\rangle$  are given by

$$\mathcal{T}_\alpha = \left\langle \left| A_\alpha^{(a)} + A_\alpha^{(b)} \right|^2 + \left| A_\alpha^{(c)} \right|^2 \right\rangle_\varepsilon, \quad \alpha = \uparrow, \downarrow \quad (8)$$

Here  $\langle \dots \rangle_\varepsilon$  stands for thermal averaging. Index (a) corresponds to processes without backscattering (see, Fig. 3a and Fig. 4a for such processes with spin  $\uparrow$  and  $\downarrow$ , respectively). Index (b) corresponds to the paths with two backscattering events (see, Fig. 3b for  $\alpha = \uparrow$  and Fig. 4b for  $\alpha = \downarrow$ ). Finally, contributions marked by (c) describes spin-flip processes with a single backscattering act (Fig. 3c and Fig. 4c for different spin polarizations). As seen from Eq. (8), the processes in which the outgoing spin polarization is parallel to the incoming one [processes (a) and (b)] interfere, while spin-flip processes (c) decouple. Notice that both  $\mathcal{T}_\uparrow$  and  $\mathcal{T}_\downarrow$  depend on position of impurity. Hence,  $\mathcal{T}_\uparrow \neq \mathcal{T}_\downarrow$ .

One can calculate transmission coefficient by direct summation of amplitudes of processes shown in Figs. 3 and 4 with the subsequent thermal averaging. This calculation is straightforward and is similar to calculation of tunneling conductance of AB interferometer made of conventional materials under the condition (1) [45], [46]. We thus relegate it to Appendix . The result reads

$$\mathcal{T} = \frac{2\gamma}{1 + \gamma^2} - \frac{16\gamma^3 A_\gamma \theta^2}{1 - \cos(4\pi\phi) + 32\gamma^2 B_\gamma}. \quad (9)$$

Here we expressed tunneling amplitudes  $r$  and  $t$  in terms of  $\gamma$  [see Eq. (4)] and introduced coefficients

$$A_\gamma = \frac{1 + 6\gamma^2 + \gamma^4}{(1 + \gamma^2)(1 - \gamma^2)^4}, \quad B_\gamma = \frac{(1 + \gamma^2)^2}{(1 - \gamma^2)^4}, \quad (10)$$

which both depend solely on the tunneling transparency. Equation (9) gives the transmission coefficient for arbitrary tunneling coupling to the leads and weak coupling to magnetic impurity. The latter is taken into account perturbatively. We see that impurity induces dependence of  $\mathcal{T}$  on the flux.

Let us consider the limiting cases of Eq. (9). The strong tunneling coupling (almost open ring with  $r \rightarrow 1$ ,  $t \rightarrow 0$ ) corresponds to  $\gamma \rightarrow 1$ , see Eq. (4). From Eq. (9) we see that the dependence on magnetic flux in this case is very weak:

$$\mathcal{T} \approx 1 - \delta\mathcal{T} - \theta^2 t^4 \cos(4\pi\phi), \quad \text{for } t \rightarrow 0. \quad (11)$$

where  $\delta\mathcal{T} \approx \theta^2/2 + 2t^2$  is flux-independent correction. Hence, for strong tunneling coupling the magnetic impurity leads to a small correction smoothly dependent on  $\phi$ . This dependence is similar to harmonic dependence

on the AB phase predicted in Ref. [30] for  $T = 0$  and slightly different geometry of the setup.

By contrast, in the opposite case of almost closed ring weakly coupled to the leads, i.e.  $\gamma \rightarrow 0$ , the dependence on the flux is very sharp:

$$\mathcal{T} \approx 2\gamma \left[ 1 - \frac{8\gamma^2\theta^2}{1 - \cos(4\pi\phi) + 32\gamma^2} \right], \quad \text{for } \gamma \rightarrow 0. \quad (12)$$

We see that  $\mathcal{T}$  shows narrow antiresonances as a function of  $\phi$  of width  $\sim \gamma$  at  $\phi = n$  and  $\phi = n + 1/2$ . Equation (12) is valid for arbitrary  $\phi$  provided that  $\theta \ll \gamma \ll 1$ . In the vicinity of the resonances,  $\delta\phi = \phi - n \ll 1$  or  $\delta\phi = \phi - (n + 1/2) \ll 1$ , one may obtain non-perturbative in  $\theta$  solution which is valid for  $\theta \ll 1$  and arbitrary relation between  $\gamma$  and  $\theta$  (see Appendix):

$$\mathcal{T} \approx 2\gamma \left[ 1 - \frac{\theta^2}{4} \frac{\gamma^2}{\gamma^2 + (\pi\delta\phi/2)^2 + (\theta/4)^2} \right]. \quad (13)$$

Thus, the non-perturbative effects lead to appearance of the additional contribution  $\theta^2/16$  in the denominator of the resonant term in (13). Physically, this corresponds to the broadening of the antiresonances because of multiple coherent scattering events.

We thus find that the transmission coefficient and, consequently, the conductance,  $G = G(\phi)$ , have minima at  $\phi = n/2$ , and maxima at  $\phi = 1/4 + n/2$  with integer  $n$ . Instead of  $G(\phi)$  it is convenient to introduce the following normalized function

$$g(\phi) = \frac{G(\phi) - G(0)}{G(1/4) - G(0)}. \quad (14)$$

which is plotted in Fig. 5.

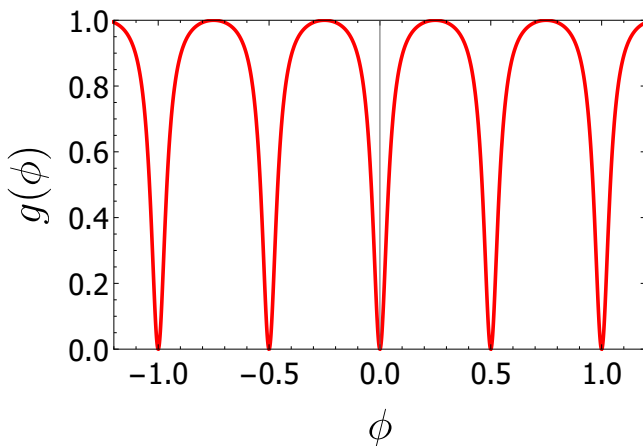


FIG. 5: The sharp antiresonances in the normalized conductance  $g(\phi)$ , Eq. (14).

We see that transmission coefficients is universal in a sense that it does not depend on details of the setup. Such universality demands for a clear physical explanation. Although the Berry's phase containing information

about structure of the helical edges drops out under condition (1), as we explained above in the end of Sec. II, one also needs to explain why the conductance is exactly periodic with the period  $1/2$  and does not depend on the position of the magnetic impurity and relation between  $L_1$  and  $L_2$ . The next section is devoted to clarification of this issue.

#### IV. PHYSICAL INTERPRETATION: COHERENT ENHANCEMENT OF THE SCATTERING OFF MAGNETIC IMPURITY

In this Section, we demonstrate that the obtained result can be derived by taking into account the coherent enhancement of backward scattering by magnetic impurity at integer and half-integer values of  $\phi$ , which is accompanied by a decrease of backward scattering (or, equivalently, increase of the forward scattering) at other values of the flux. The effect is fully analogous to coherent enhancement of backscattering caused by weak localization (see Ref. [67] for review). As we will see, this analogy significantly helps to explain universality of the result.

This analogy can be clarified by analyzing Figs. 3 and 4. Trajectories (a) and (b) with equal  $n$  contain a loop (marked by red color) where both trajectories start from magnetic impurity and make  $n$  full revolutions in the opposite directions, clockwise for the trajectory (a) and counterclockwise for the trajectory (b). This is the typical weak localization loop. The only essential difference as compared to weak localization in disordered diffusive systems is that in the case of helical edges the returns to impurity are ballistic. As illustrated in Figs. 3c and 4c, two spin-flip processes with a given winding number but different sequence of backward and forward scattering events can also contain a closed loop (marked by red color) passed in the opposite directions. Two processes where a closed loop is passed in the opposite directions have equal lengths and the same final spins, so that they interfere and the corresponding flux-sensitive interference contribution is not affected by the thermal averaging.

Let us now demonstrate that the quantum correction to the conductance is *fully* determined by the "weak localization" processes. The simplest way to do this is to use the approach of Ref. [68], where it was shown that the effect of weak localization in 2D electron gas can be fully incorporated into the renormalization of the classical differential cross-section on a single impurity. Hence, one can describe weak localization effect by classical Drude-Boltzmann equation with the differential cross-section renormalized by the quantum correction. The latter is proportional to the so-called Cooperon, which is given by the sum of the maximally crossed diagrams.

Next, we demonstrate that a similar description is applicable to our problem. To this end, we first consider transport in our setup within the classical approximation, which implies that the magnetic impurity is described by

the forward and backward scattering probabilities:

$$t_f^0 = \cos^2 \theta, \quad t_b^0 = \sin^2 \theta. \quad (15)$$

The classical transmission coefficient can be presented as the sum over contributions from classical trajectories propagating clockwise and counterclockwise and experience collisions with probabilities (15). In the perturbative regime, the result reads (see Appendix)

$$\mathcal{T}_{cl} \approx \frac{2\gamma}{1 + \gamma^2} - \frac{2\gamma^2\theta^2}{(1 + \gamma^2)^2}. \quad (16)$$

This equation does not contain contribution from interfering trajectories and, hence, is flux-independent. One can check that it can be obtained from Eq. (9) for quantum transmission coefficient by averaging over the flux:

$$\mathcal{T}_{cl} = \langle \mathcal{T} \rangle_\phi. \quad (17)$$

As a next step, we will show that the difference between quantum and classical results [Eq. (9) and Eq. (16), respectively] can be *fully* expressed in terms of quantum weak localization corrections to the classical scattering probabilities  $t_f^0$  and  $t_b^0$ . The latter describe single scattering processes by magnetic impurity shown in the left panels of Figs. 6 (a) and (b), respectively. Let us consider two processes involving multiple scattering by magnetic impurity after some number of ballistic returns. First process is shown in Fig. 6a (right panel) and describes the first order quantum correction to  $t_f^0$ . The first order correction to the probability of the backward scattering is shown in the right panel of Fig. 6 (b). Both processes involve ballistic returns to the magnetic impurity after a number of revolutions around the ring in which the electron wave splits into two parts passing the setup in the opposite directions with equal winding numbers. Summing over winding numbers, we find “ballistic Cooperon”

$$\mathcal{C} = \frac{t^4 e^{4i\pi\phi}}{1 - t^4 \cos^2 \theta e^{4i\pi\phi}} + \frac{t^4 e^{-4i\pi\phi}}{1 - t^4 \cos^2 \theta e^{-4i\pi\phi}}, \quad (18)$$

which represents the contribution of the processes shown in Fig 6(c). Notice that

$$\langle \mathcal{C} \rangle_\phi = 0. \quad (19)$$

One can easily calculate contributions from these processes to scattering probabilities

$$\delta t_f = -\cos^2 \theta \sin^2 \theta \mathcal{C}, \quad \delta t_b = \cos^2 \theta \sin^2 \theta \mathcal{C}. \quad (20)$$

As seen, these equations obey probability conservation law:

$$\delta t_f + \delta t_b = 0. \quad (21)$$

The total scattering probabilities incorporating first order quantum corrections read

$$t_f = t_f^0 + \delta t_f, \quad t_b = t_b^0 + \delta t_b. \quad (22)$$

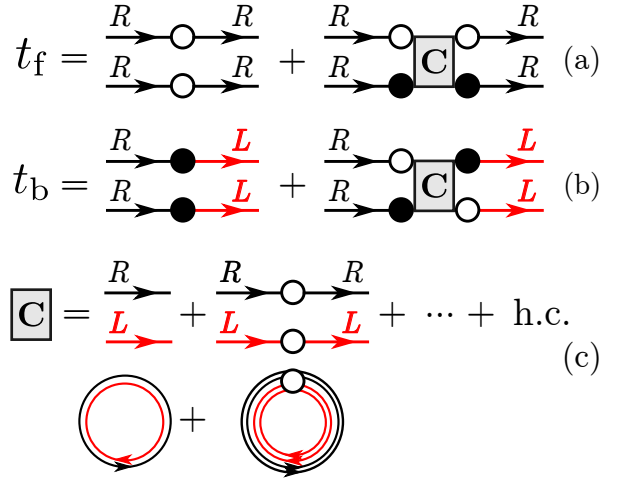


FIG. 6: Forward (a) and backward (b) single scattering events [left panels of (a) and (b), respectively] and coherent scattering processes [right panels of (a) and (b)] leading to enhancement of scattering probabilities due to ballistic returns to the magnetic impurity. Probabilities of both coherent processes are proportional to the ballistic Cooperon (c) which is given by the sum over closed ballistic loops formed by trajectories propagating in the opposite directions and having different winding numbers. Open circles and black dots describe amplitudes of single forward and backward scattering events, respectively. The contributions of coherent processes [right (a) and (b) panels] coincide by absolute value, while the phase factor  $i$  arising in each backscattering act enters in different way,  $\delta t_f = \cos^2 \theta (-i \sin \theta)^2 \mathcal{C}$ ,  $\delta t_b = \cos^2 \theta (i \sin \theta) (-i \sin \theta) \mathcal{C}$ , which ensures the probability conservation:  $\delta t_f + \delta t_b = 0$ .

In the limit of small  $\theta$ , from Eqs. (18) and (20) we find

$$\delta t_b \approx \theta^2 \mathcal{C}|_{\theta=0}. \quad (23)$$

Since  $t_b^0 \simeq \theta^2$  at small  $\theta$ , see Eq. (15), the total factor appearing due to the coherent scattering is given by

$$\frac{t_b}{t_b^0} \approx 1 + \mathcal{C}|_{\theta=0} = \frac{8\gamma(1 + \gamma^2)^2 A_\gamma}{32\gamma^2 B_\gamma + 1 - \cos(4\pi\phi)}, \quad (24)$$

where  $A_\gamma$  is given by Eq. (10). For  $\gamma \ll 1$ , this equation becomes

$$\frac{t_b}{t_b^0} \approx \frac{8\gamma}{32\gamma^2 + 1 - \cos(4\pi\phi)}. \quad (25)$$

Exactly at the resonances, the backscattering probability is enhanced by the factor

$$\left( \frac{t_b}{t_b^0} \right)_{\max} = \frac{1}{4\gamma} \gg 1, \quad (26)$$

as compared to the classical backward probability. On the other hand, the classical backscattering probability is suppressed beyond the resonance region. The dependence  $t_b(\phi)$  is shown in Fig. 7.

The dependence of the quantum conductance  $\mathcal{T}$  on  $\phi$  at  $\theta \rightarrow 0$  is obtained by replacing  $\theta^2$  in the classical

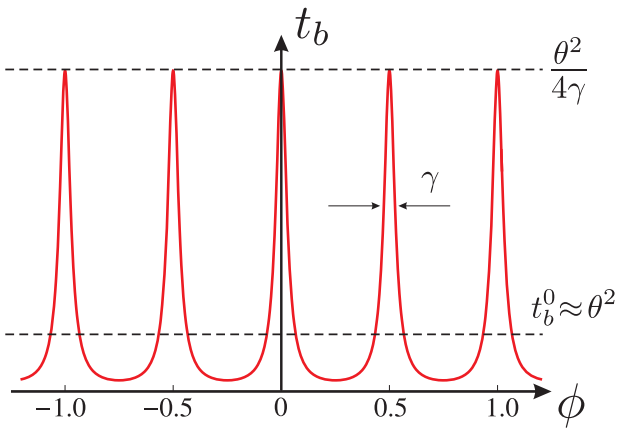


FIG. 7: Dependence of total backscattering probability  $t_b$  on magnetic flux for weak tunneling coupling ( $\gamma \ll 1$ ). This probability is strongly enhanced in the vicinity of the resonances and suppressed outside resonance region as compared to the classical flux-independent probability  $t_b^0$  shown by dashed line.

expression, Eq. (16), with its renormalized value  $\theta^2 \rightarrow \theta^2 (t_b/t_b^0) = \theta^2(1 + \mathcal{C}|_{\theta=0})$ . Evidently, the relation (17) is fulfilled due to Eq. (19).

Concluding here, we observe that the effective backward scattering is dramatically enhanced in vicinity of integer and half-integer values of the magnetic flux and is suppressed at other values of the flux.

Based on derivation presented above, we can now explain the universal behavior of the conductance. The universality is due to several physical reasons:

- Multiple returns to magnetic impurity—the effect responsible for coherent enhancement of magnetic disorder—are only sensitive to the total length of the edge and independent of other details of the interferometer, e.g., to relation between  $L_1$  and  $L_2$  and position of the magnetic impurity.
- The exact periodicity of the conductance with the period  $1/2$  is a specific property of weak localization in a systems where the area covered by the return loops is fixed with the precision higher than the squared magnetic length [2].
- The Berry's phase, which encodes information about geometry of the setup drops out from the high-temperature transmission coefficient.

Actually, first two statements in this list are less trivial than it seems at first glance. The key point here is the absence of backscattering by non-magnetic contacts in helical edge. Due to this property the quantum correction to the conductance can be *fully* expressed in terms of weak localization correction. For non-helical interferometers, where backscattering on contacts is inevitable, there are other interference contributions which are not

described in terms of weak localization correction and lead to the violation of periodicity with the period  $1/2$  [69].

## V. DEPHASING INDUCED BY DYNAMICS OF MAGNETIC IMPURITY

One of the key problems related to efficiency of any interferometer is the dephasing caused by inelastic processes. Here we briefly discuss one of the possible mechanisms of dephasing. A more detailed analysis will be presented elsewhere [63].

The dominating mechanism of dephasing in low dimensional systems is usually connected with the electron-electron interaction. For tunneling AB interferometers made of conventional (non-helical) single-channel ballistic wires, the effect of interaction for  $T \gg \Delta$  was studied in Ref. [45] (see also Refs. [47], [48]). It was found that antiresonances in the dependence  $G(\phi)$  split into a series of narrow peaks separated by distance  $\alpha$  with a smooth envelope of the width  $\alpha\sqrt{T/\Delta}$ , where  $\alpha$  is the dimensionless interaction constant. Each peak is broadened by dephasing within the width  $\gamma T/\Delta$ , which turns out to be interaction-independent and gets suppressed with closing the interferometer ( $\gamma \rightarrow 0$ ). The underlying physics is related to interaction of the tunneling electrons with so-called zero-mode fluctuations, i.e. tunneling-induced fluctuations of total numbers of right- and left-moving electrons,  $N_R$  and  $N_L$ , respectively.

Similar dephasing would also occur in the case under discussion [71]. There is however, a competing contribution to dephasing caused by chaotic dynamics of impurity moment  $\mathbf{M}$ . The latter mechanism can be more effective in an almost closed interferometer of sufficiently large size  $L$ . The random behavior of  $\mathbf{M}(t)$  can occur for a number of reasons. First of all, the dynamics of  $\mathbf{M}(t)$  appears due to the exchange interaction with the thermal bath of electrons in the helical edge modes. This mechanism was recently discussed in Refs. [36] for the case of infinite edge, where a general equation for relaxation of averaged moment  $\langle \mathbf{M}(t) \rangle$  was derived. Simple estimates show that for a ring-shaped edge of finite length  $L$  weakly coupled to thermalized leads the theory developed in [36] should be essentially modified. Most importantly, zero mode fluctuations come into play and dramatically change the dephasing action in close analogy with the effect of the electron-electron interaction [45]. This would lead to a non-trivial dynamics of  $\mathbf{M}(t)$ .

Here, we confine ourselves to the analysis of much simpler mechanism, namely, we assume that a slow random dynamics of  $\mathbf{M}(t)$  is caused by the interaction with external magnetic bath, in particular, with thermal bath of bulk magnetic impurities. We also assume that this bath is isotropic, so that the correlation function describing the magnetic moment relaxation is given by

$$\langle M_\alpha(0)M_\beta(t) \rangle = \frac{M^2}{3} \delta_{\alpha\beta} e^{-\Gamma t}, \quad (27)$$



where  $\Gamma$  is the isotropic relaxation rate.

The dephasing rate caused by relaxation (27) can be calculated as follows. We assume that the electron spin at the position of the magnetic impurity is directed along the  $\hat{z}$  axis, and the components of the classical vector  $\mathbf{M}$  are given by:  $M_z = M \cos \chi$ ,  $M_x = M \sin \chi \cos \varphi$ ,  $M_y = M \sin \chi \sin \varphi$ . A slow evolution of  $\mathbf{M}(t)$  is encoded in the time dependence of angles  $\chi = \chi(t)$  and  $\varphi = \varphi(t)$ . For fixed values of  $\chi$  and  $\varphi$  the scattering matrix  $\hat{S}_M$  is given by Eq. (7) with  $\theta = gM \sin \chi$ , where  $g \ll 1$  is the exchange coupling constant. Let us discuss the simplest situation, when the scattering on magnetic impurity is considered in the lowest order with respect to  $\theta$ , whereas  $\chi$  is arbitrary. The correction to the backscattering for static impurity is given in this case by Eq. (23). In order to take into account the slow dynamics of  $\mathbf{M}$  this equation should be modified as follows:

$$\delta t_b = 2\text{Re} \sum_{n=0}^{\infty} (t^4 e^{4i\pi\phi})^{n+1} \left\langle \theta(0)\theta(t_n) e^{i(\varphi(0) - \varphi(t_n))} \right\rangle, \quad (28)$$

where  $t_n = 2\pi n/\Delta$ . Next, we notice that  $\langle \theta(0)\theta(t_n) e^{i(\varphi(0) - \varphi(t_n))} \rangle = g^2 \langle M_+(0)M_-(t) \rangle$  (with  $M_{\pm} = M_x \pm iM_y$ ) and use Eq. (27). For  $\Gamma \ll \Delta$  and  $\gamma \ll 1$ , we find that Eq. (9) becomes

$$\mathcal{T} \approx 2\gamma - \frac{16\gamma^3 \langle \theta^2 \rangle}{1 - \cos(4\pi\phi) + 32(\gamma + \gamma_{\varphi})^2}, \quad (29)$$

where

$$\gamma_{\varphi} = \frac{\pi\Gamma}{4\Delta} \quad (30)$$

is the dimensionless dephasing rate and  $\langle \theta^2 \rangle = g^2 M^2 \langle \sin^2 \chi \rangle = 2g^2 M^2/3$ . The dephasing given by Eq. (30) should dominate over interaction-induced one provided that relaxation rate  $\Gamma$  is large as compared to interaction-induced splitting of antiresonances:  $\Gamma \gg \alpha\sqrt{T\Delta}$ .

## VI. CONCLUSIONS

We studied the transport through the tunneling Aharonov-Bohm interferometer formed by helical edge states in the presence of a magnetic impurity. We demonstrated that at relatively high temperatures,  $T \gg \Delta$  (which, for typical values of parameters, corresponds to temperatures higher than several kelvins), the tunneling conductance of the interferometer shows sharp antiresonances. The antiresonances are separated by distance  $\Delta\phi = 1/2$ , which means that the tunneling conductance is periodic function of the magnetic flux with the period given by half of the flux quantum. They are universal in a sense that their shape and position are not sensitive to geometry of the setup and to the position of the magnetic impurity. We interpret this universal resonant behavior as a coherent enhancement of backward scattering off

magnetic impurity at integer and half-integer values of flux, which is accompanied by suppression of the effective scattering at other values of flux. Both enhancement and suppression are due to the interference of processes involving multiple returns (clockwise and counterclockwise) to magnetic impurity after revolutions around interferometer circumference — the phenomenon similar to weak-localization-induced enhancement of backscattering.

A very sharp dependence of the conductance is very promising in view of possible applications in the area of extremely sensitive detectors of magnetic fields. Most importantly, the predicted dependence of the effective scattering probability on the magnetic flux allows for flux-tunable control of the magnetic disorder.

## VII. ACKNOWLEDGEMENTS

The work of R.N. and V.K. was supported by the joint grant of the Russian Science Foundation (Grant No. 16-42-01035) and the Deutsche Forschungsgemeinschaft (Grant No. MI 658-9/1).

### Appendix: Technical details of calculations

#### a. Classical conductance

The classical conductance of the interferometer with a magnetic impurity can be presented as a following sum:

$$\mathcal{T}_{\text{cl}} = \frac{r^4}{2} \sum_{n=0}^{\infty} [J_1^{(n)} + J_2^{(n)}]. \quad (\text{A.1})$$

Here  $J_1^{(n)}$  ( $J_2^{(n)}$ ) is the classical current, corresponding to particle which exit the interferometer through the right contact moving clockwise (counterclockwise) after passing this contact  $n$  times without scattering to the lead. Having in mind that the impurity is placed in the upper shoulder of the interferometer (see Fig. 1), one can easily find the following set of the recurrent equations for classical currents  $J_{1,2}^{(n)}$ :

$$\mathbf{J}^{(n+1)} = \begin{pmatrix} t^4 \cos^2 \theta & t^2 \sin^2 \theta \\ t^6 \sin^2 \theta & t^4 \cos^2 \theta \end{pmatrix} \mathbf{J}^{(n)} \quad (\text{A.2})$$

with  $\mathbf{J}^{(n)} = (J_1^{(n)}, J_2^{(n)})$  and  $\mathbf{J}^{(0)} = (\cos^2 \theta, 1 + t^2 \sin^2 \theta)$ .

Solving these equations, expressing  $r$  and  $t$  via  $\gamma$  [see Eq. (4)], we find

$$\mathcal{T}_{\text{cl}} = 2\gamma \frac{4\gamma + (\gamma^2 - 4\gamma + 1) \sin^2 \theta}{4\gamma(1 + \gamma^2) + (1 - \gamma)^4 \sin^2 \theta}. \quad (\text{A.3})$$

Expanding the result up to the second order with respect to  $\theta$ , we arrive at Eq. (16) of the main text.

Next, we calculate quantum conductance in two different cases: the very weak magnetic impurity when calculations can be done perturbatively with respect to  $\theta$  and the case when the magnetic impurity is relatively strong.

*b. Perturbative quantum analysis*

Here, we calculate sum of the amplitudes corresponding to the processes shown in Figs. 3 and 4. The energy dependence appears in the transmission amplitudes via the factor  $\exp[i(kL + \delta)]$ . Due to the condition  $T \gg \Delta$ , this exponent rapidly oscillates when energy changes within the temperature window around the Fermi energy. To the exponential precision, one can thus replace the energy averaging by the averaging over the phase  $\varphi = kL + \delta$  within the interval  $0 < \varphi < 2\pi$ . Already on this stage the Berry's phase drops out. Next one can replace  $\exp(i\varphi) = z$  and reduce the averaging over  $\varphi$  to the calculation of contour integral over  $z$ . In all considered cases the integrand in appearing integrals has a simple pole structure and can be easily evaluated.

We start with deriving some auxiliary equations which allow one to perform thermal averaging. For any  $a$  such that  $|a| < 1$  and any analytical function  $F(z)$ , we have

$$\left\langle \frac{F(e^{i\varphi})}{1 - ae^{-i\varphi}} \right\rangle_{\varphi} = F(a), \quad (\text{A.4})$$

Using this equation, we find for any  $b$  ( $|b| < 1$ ) and  $c$  ( $|c| < 1$ ):

$$\begin{aligned} & \left\langle \frac{e^{in\varphi}}{(1 - ae^{-i\varphi})(1 - be^{i\varphi})(1 - ce^{i\varphi})} \right\rangle_{\varphi} \\ &= \frac{a^n}{(1 - ba)(1 - ca)}, \end{aligned} \quad (\text{A.5})$$

and

$$\begin{aligned} & \left\langle \left| \frac{1}{1 - ae^{-i\varphi}} \right|^2 \left| \frac{1}{1 - be^{-i\varphi}} \right|^2 \right\rangle_{\varphi} \\ &= \frac{1 - |a|^2|b|^2}{(1 - |a|^2)(1 - |b|^2)|1 - b^*a|^2}. \end{aligned} \quad (\text{A.6})$$

The summation of amplitudes of different interference processes can be obtained perturbatively in  $\theta$  provided that  $\theta \ll \max(\gamma, 1)$ . The tunneling amplitudes of trajectories shown in Fig. 3a,b are given, respectively, by the following equations

$$\begin{aligned} A_{\uparrow}^{(a)} &= \frac{r^2 \cos \theta e^{i\varphi_+ L_1/L}}{1 - t^2 \cos \theta e^{i\varphi_+}}, \\ A_{\uparrow}^{(b)} &= \frac{r^2 t^2 (i \sin \theta)^2 e^{i(\varphi_- + \varphi_+ L_1/L)}}{[1 - t^2 \cos \theta e^{i\varphi_+}]^2 [1 - t^2 \cos \theta e^{i\varphi_-}]}, \end{aligned} \quad (\text{A.7})$$

which are obtained by direct summation of tunneling amplitudes with different winding numbers. Here

$$\varphi_{\pm} = kL \pm 2\pi\phi \quad (\text{A.8})$$

(we incorporated the Berry's phase into the dynamical phase). The factor  $[1 - t^2 \cos \theta e^{i\varphi_+}]^{-1}$  in  $A_{\uparrow}^{(a)}$  appears due to summation of contributions of clockwise rotating ballistic trajectories over winding number  $n$ . The denominator in  $A_{\uparrow}^{(b)}$  stems from contributions of clockwise processes with different winding numbers both before and after backscattering, together with contributions of counterclockwise scattering processes between two backscattering acts.

The amplitude of the process shown in Fig. 3c reads

$$A_{\uparrow}^{(c)} = \frac{r^2 t (i \sin \theta) e^{i[\varphi_+ s/L + \varphi_- (L+s-L_1)/L]}}{[1 - t^2 \cos \theta e^{i\varphi_+}][1 - t^2 \cos \theta e^{i\varphi_-}]}, \quad (\text{A.9})$$

where  $s$  is the distance from the left contact to the impurity position.

The processes with opposite incoming spin are shown in Fig. 4. The analytical expressions for corresponding amplitudes read

$$\begin{aligned} A_{\downarrow}^{(a)} &= \frac{r^2 e^{i\varphi_- (L-L_1)/L}}{1 - t^2 \cos \theta e^{i\varphi_-}}, \\ A_{\downarrow}^{(b)} &= \frac{r^2 t^4 (i \sin \theta)^2 e^{i(\varphi_+ + \varphi_- (2L-L_1)/L)}}{[1 - t^2 \cos \theta e^{i\varphi_-}]^2 [1 - t^2 \cos \theta e^{i\varphi_+}]}, \\ A_{\downarrow}^{(c)} &= \frac{r^2 t (i \sin \theta) e^{i[\varphi_+ (L_1-s)/L + \varphi_- (L-s)/L]}}{[1 - t^2 \cos \theta e^{i\varphi_+}][1 - t^2 \cos \theta e^{i\varphi_-}]}, \end{aligned} \quad (\text{A.10})$$

Substituting Eqs. (A.7), (A.9), and (A.10) into Eqs. (8), performing energy averaging with the use of Eqs. (A.4), (A.5), and (A.6), expanding results over  $\theta$  up to the second order and using Eq. (5), we find after some algebra Eq. (9) of the main text.

*c. Non-perturbative quantum analysis*

For weak tunneling coupling,  $\gamma \ll 1$ , one can derive non-perturbative in  $\theta$  equation for transmission coefficient, which is valid for arbitrary relation between  $\theta$  and  $\gamma$  (but it is still assumed that  $\theta \ll 1$ ). To this end, one can use an approach developed in [46, 62] for conventional (non-helical) interferometers. For simplicity, we only consider the case of the interferometer with equal shoulders:  $L_1 = L_2$ .

The electron tunneling transmission amplitude is a matrix  $\hat{t} = \hat{t}(\epsilon)$  in a spin space with elements  $t_{\alpha\beta} = \langle \alpha | \hat{t} | \beta \rangle$ . The transmission coefficient is expressed in terms of this amplitude as follows:

$$\mathcal{T}(\epsilon) = \frac{1}{2} \text{Tr} \hat{t} \hat{t}^\dagger. \quad (\text{A.11})$$

The tunneling trajectory with  $n$  full revolutions around the setup has a length  $L_n = L(n+1/2)$ . The transmission amplitude can be expressed as a sum over  $n$ :

$$\hat{t}(\epsilon) = \sum_{n=0}^{\infty} \hat{\beta}_n e^{ikL_n}. \quad (\text{A.12})$$

The quantity  $\hat{\beta}_n$  consists of two contributions: trajectories ending at the bottom semicircle,  $\hat{\beta}_n^+$  and at the top semicircle,  $\hat{\beta}_n^-$ . The vector constructed out of these two contributions,

$$\vec{\beta}_n = \begin{pmatrix} \hat{\beta}_n^+ \\ \hat{\beta}_n^- \end{pmatrix}, \quad (\text{A.13})$$

obeys a recurrence relation

$$\vec{\beta}_{n+1} = \hat{A}\vec{\beta}_n,$$

where  $\hat{A}$  is certain  $n$ -independent matrix. Then,  $\vec{\beta}_n$  is given by  $\hat{\beta}_n = \vec{e}\hat{A}^n\vec{\beta}_0$ , where

$$\vec{e} = \begin{pmatrix} \mathbf{1} \\ \mathbf{1} \end{pmatrix}. \quad (\text{A.14})$$

The transmission coefficient,

$$\mathcal{T}(\epsilon) = \frac{1}{2}\text{Tr} \sum_{n,m=0}^{\infty} \hat{\beta}_n \hat{\beta}_m^\dagger e^{ik(L_n - L_m)}, \quad (\text{A.15})$$

after energy averaging under condition  $T \gg \Delta$  has only nonzero terms with  $n = m$  and is expressed in terms of matrix  $\hat{A}$  as follows

$$\mathcal{T} = \frac{1}{2}\text{Tr} \sum_{n=0}^{\infty} |\hat{\beta}_n|^2 = \frac{1}{2}\text{Tr} \sum_{n=0}^{\infty} |\vec{e}\hat{A}^n\vec{\beta}_0|^2. \quad (\text{A.16})$$

Calculation of the sum (see technical details in Refs. [46, 62]) yields a matrix  $\hat{B} = (\mathbf{1} - \hat{A} \otimes \hat{A}^\dagger)^{-1}$  acting in the space of doubled dimension. Hence, the problem is reduced to a straightforward (albeit cumbersome) calculation of matrix elements of  $\hat{B}$ .

Because of the helical nature of the edge state the matrix  $\hat{A}$  is simplified since we assume that counterclockwise electron propagation mode with the spin up as well as clockwise mode with spin down are absent:

$$\hat{A} = \begin{pmatrix} 0 & 0 & 0 & 0 \\ 0 & -e^{2i\pi\phi t^2} \cos \theta & -e^{2iks t^3} \sin \theta & 0 \\ 0 & e^{-2iks t} \sin \theta & -e^{-2i\pi\phi t^2} \cos \theta & 0 \\ 0 & 0 & 0 & 0 \end{pmatrix}. \quad (\text{A.17})$$

The initial amplitudes read

$$\begin{aligned} \hat{\beta}_0^+ &= \begin{pmatrix} 0 & 0 \\ -e^{i\pi\phi}(1-t^2) & -e^{2iks+i\pi\phi}t(1-t^2)\sin\theta \end{pmatrix}, \\ \hat{\beta}_0^- &= \begin{pmatrix} 0 & -e^{-i\pi\phi}(1-t^2)\cos\theta \\ 0 & 0 \end{pmatrix}. \end{aligned} \quad (\text{A.18})$$

Using these formula, one can represent the transmission coefficient as a ratio of two rather cumbersome functions of  $\theta, \gamma$  and  $\delta\phi$ . In the limit  $\theta, \gamma, \delta\phi \ll 1$ , one can expand both functions over  $\theta, \gamma$  and  $\delta\phi$  up to the terms of second order. Doing so, we arrive at Eq. (13) of the main text. One can show that this equation is also valid for  $L_1 \neq L_2$ .

- 
- [1] Y. Aharonov and D. Bohm, *Phys. Rev.* **115**, 485 (1959).  
[2] A. G. Aronov and Y. V. Sharvin, *Rev. Mod. Phys.* **59**, 755 (1987).  
[3] C. L. Kane and E. J. Mele, *Phys. Rev. Lett.* **95**, 226801 (2005).  
[4] C. L. Kane and E. J. Mele, *Phys. Rev. Lett.* **95**, 146802 (2005).  
[5] B. A. Bernevig, T. L. Hughes, and S.-C. Zhang, *Science* **314**, 1757 (2006).  
[6] M. König, S. Wiedmann, C. Brune, A. Roth, H. Buhmann, L. W. Molenkamp, X.-L. Qi, and S.-C. Zhang, *Science* **318**, 766 (2007).  
[7] A. Roth, C. Brüne, H. Buhmann, L. W. Molenkamp, J. Maciejko, X.-L. Qi, S.-C. Zhang, *Science* **325**, 294 (2009).  
[8] G. M. Gusev, Z. D. Kvon, O. A. Shegai, N. N. Mikhailov, S. A. Dvoretzky, J. C. Portal, *Phys. Rev. B* **84**, 121302(R) (2011).  
[9] C. Brüne, A. Roth, H. Buhmann, E. M. Hankiewicz, L. W. Molenkamp, J. Maciejko, X.-L. Qi, S.-C. Zhang, *Nature Phys.* **8**, 485 (2012).  
[10] A. Kononov, S. V. Egorov, Z. D. Kvon, N. N. Mikhailov, S. A. Dvoretzky, E. V. Deviatov, *JETP Lett.* **101**, 814 (2015).  
[11] M. Z. Hasan and C. L. Kane, *Rev. Mod. Phys.* **82**, 3045 (2010).  
[12] Xiao-Liang Qi and Shou-Cheng Zhang, *Rev. Mod. Phys.* **83**, 1057 (2011).  
[13] R.-L. Chu, J. Li, J. K. Jain, and S.-Q. Shen, *Phys. Rev. B* **80**, 081102 (2009).  
[14] D. Hsieh, Y. Xia, D. Qian, L. Wray, J. H. Dil, F. Meier, J. Osterwalder, L. Patthey, J. G. Checkelsky, N. P. Ong, et al., *Nature* **460**, 1101 (2009).  
[15] J. H. Bardarson, P. W. Brouwer, and J. E. Moore, *Phys. Rev. Lett.* **105**, 156803 (2010).  
[16] H. Peng, K. Lai, D. Kong, S. Meister, Y. Chen, X.-L. Qi, S.-C. Zhang, Z.-X. Shen, and Y. Cui, *Nat Mater* **9**, 225 (2010).  
[17] P. Michetti and P. Recher, *Phys. Rev. B* **83**, 125420 (2011).  
[18] P. Delplace, J. Li, and M. Büttiker, *Phys. Rev. Lett.* **109**, 246803 (2012).  
[19] S. Masuda and Y. Kuramoto, *Phys. Rev. B* **85**, 195327 (2012).  
[20] J. H. Bardarson and J. E. Moore, *Reports on Progress in Physics* **76**, 056501 (2013).  
[21] N. Kainaris, I. V. Gornyi, S. T. Carr, and A. D. Mirlin, *Phys. Rev. B* **90**, 075118 (2014).  
[22] E. B. Olshanetsky, Z. D. Kvon, G. M. Gusev, A. D. Levin, O. E. Raichev, N. N. Mikhailov, and S. A. Dvoretzky, *Phys. Rev. Lett.* **114**, 126802 (2015).  
[23] P. Dutta, A. Saha, and A. M. Jayannavar, *Physical Review B* **94**, 195414 (2016).  
[24] B.-C. Lin, S. Wang, L.-X. Wang, C.-Z. Li, J.-G. Li, D. Yu, and Z.-M. Liao, *Phys. Rev. B* **95**, 235436 (2017).

- [25] N. Kainaris, I. V. Gornyi, A. Levchenko, and D. G. Polyakov, *Phys. Rev. B* **95**, 045150 (2017).
- [26] G.M. Gusev, Z.D. Kvon, O.A. Shegai, N.N. Mikhailov, S.A. Dvoretzky, *Solid.State Commun.* **205**, 4 (2015).
- [27] L. Du, I. Knez, G. Sullivan, and R.-R. Du, *Phys. Rev. Lett.* **114**, 096802 (2015).
- [28] S.-B. Zhang, Y.-Y. Zhang, and S.-Q. Shen, *Phys. Rev. B* **90**, 115305 (2014).
- [29] L.-H. Hu, D.-H. Xu, F.-C. Zhang, and Y. Zhou, *Phys. Rev. B* **94**, 085306 (2016).
- [30] F. Dolcini, *Phys. Rev. B* **83**, 165304 (2011).
- [31] J. I. Väyrynen, M. Goldstein, L. I. Glazman, *Phys. Rev. Lett.* **110**, 216402 (2013).
- [32] J. I. Väyrynen, M. Goldstein, Y. Gefen, L. I. Glazman, *Phys. Rev. B* **90**, 115309 (2014).
- [33] B. L. Altshuler, I. L. Aleiner, V. I. Yudson, *Phys. Rev. Lett.* **111**, 086401 (2013).
- [34] L. Kimme, B. Rosenow, A. Brataas, *Phys. Rev. B* **93**, 081301 (2016).
- [35] J. I. Väyrynen, F. Geissler, L. I. Glazman, *Phys. Rev. B* **93**, 241301(R) (2016).
- [36] P. D. Kurilovich, V. D. Kurilovich, I. S. Burmistrov, M. Goldstein, arXiv:1710.00384, unpublished
- [37] M. Büttiker, Y. Imry, and M. Y. Azbel, *Phys. Rev. A* **30**, 1982 (1984).
- [38] Y. Gefen, Y. Imry, and M. Y. Azbel, *Phys. Rev. Lett.* **52**, 129 (1984).
- [39] M. Büttiker, Y. Imry, R. Landauer, and S. Pinhas, *Phys. Rev. B* **31**, 6207 (1985).
- [40] E. A. Jagla and C. A. Balseiro, *Phys. Rev. Lett.* **70**, 639 (1993).
- [41] A. Yacoby, R. Schuster, and M. Heiblum, *Phys. Rev. B* **53**, 9583 (1996).
- [42] J. M. Kinaret, M. Jonson, R. I. Shekhter, and S. Eggert, *Phys. Rev. B* **57**, 3777 (1998).
- [43] A. van Oudenaarden, M. H. Devoret, Y. V. Nazarov, and J. E. Mooij, *Nature* **391**, 768 (1998).
- [44] D.-I. Chang, G. L. Khym, K. Kang, Y. Chung, H.-J. Lee, M. Seo, M. Heiblum, D. Mahalu, and V. Umansky, *Nature Physics* **4**, 205 (2008).
- [45] A. P. Dmitriev, I. V. Gornyi, V. Y. Kachorovskii, and D. G. Polyakov, *Phys. Rev. Lett.* **105**, 036402 (2010).
- [46] P. M. Shmakov, A. P. Dmitriev, and V. Y. Kachorovskii, *Phys. Rev. B* **87**, 235417 (2013).
- [47] A. P. Dmitriev, I. V. Gornyi, V. Y. Kachorovskii, D. G. Polyakov, and P. M. Shmakov, *JETP Letters* **100**, 839 (2015).
- [48] A. P. Dmitriev, I. V. Gornyi, V. Y. Kachorovskii, and D. G. Polyakov, *Phys. Rev. B* **96**, 115417 (2017).
- [49] Y. Aharonov and A. Casher, *Phys. Rev. Lett.* **53**, 319 (1984).
- [50] H. Mathur and A. D. Stone, *Phys. Rev. B* **44**, 10957 (1991).
- [51] H. Mathur and A. D. Stone, *Phys. Rev. Lett.* **68**, 2964 (1992).
- [52] A. G. Aronov and Y. B. Lyanda-Geller, *Phys. Rev. Lett.* **70**, 343 (1993).
- [53] D. Frustaglia and K. Richter, *Phys. Rev. B* **69**, 235310 (2004).
- [54] B. Molnár, F. M. Peeters, and P. Vasilopoulos, *Phys. Rev. B* **69**, 155335 (2004).
- [55] R. Citro and F. Romeo, *Phys. Rev. B* **73**, 233304 (2006).
- [56] R. Citro, F. Romeo, and M. Marinaro, *Phys. Rev. B* **74**, 115329 (2006).
- [57] A. A. Kovalev, M. F. Borunda, T. Jungwirth, L. W. Molenkamp, and J. Sinova, *Phys. Rev. B* **76**, 125307 (2007).
- [58] V. Moldoveanu and B. Tanatar, *Phys. Rev. B* **81**, 035326 (2010).
- [59] M. König, A. Tschetschetkin, E. M. Hankiewicz, J. Sinova, V. Hock, V. Daumer, M. Schäfer, C. R. Becker, H. Buhmann, and L. W. Molenkamp, *Phys. Rev. Lett.* **96**, 076804 (2006).
- [60] F. Nagasawa, J. Takagi, Y. Kunihashi, M. Kohda, and J. Nitta, *Phys. Rev. Lett.* **108**, 086801 (2012).
- [61] F. Nagasawa, D. Frustaglia, H. Saarikoski, K. Richter, and J. Nitta, *Nature Communications* **4**, 2526 (2013).
- [62] P. M. Shmakov, A. P. Dmitriev, and V. Y. Kachorovskii, *Physical Review B* **85**, 075422 (2012).
- [63] R. A. Niyazov, D. N. Aristov, and V. Y. Kachorovskii, to be published.
- [64] D. N. Aristov and R. A. Niyazov, *Phys. Rev. B* **94**, 035429 (2016).
- [65] D. N. Aristov, A.P. Dmitriev, I.V. Gornyi, V.Yu. Kachorovskii, D. G. Polyakov, and P. Wölffe, *Phys. Rev. Lett.* **105**, 266404 (2010).
- [66] M. V. Berry, *Proceedings of the Royal Society A: Mathematical, Physical and Engineering Sciences* **392**, 45 (1984).
- [67] S. Chakravarty and A. Schmid, *Physics Reports* **140**, 193 (1986).
- [68] A. P. Dmitriev, V. Y. Kachorovskii, and I. V. Gornyi, *Phys. Rev. B* **56**, 9910 (1997).
- [69] The backscattering destroys antiresonances in the symmetrical setup ( $L_1 = L_2$ ) at integer values of magnetic flux and restores the periodicity of the conductance with the period  $\Delta\phi = 1$  in the conventional non-helical single-channel interferometers, both ballistic [45, 70] and containing impurities [46]. In the asymmetrical setup ( $L_1 \neq L_2$ ), the antiresonances at  $\phi = n$  exist but they have different widths and amplitudes as compared to antiresonances at  $\phi = n + 1/2$  [70]. For helical-edge case, where backscattering is prohibited, the antiresonances at  $\phi = n$  and  $\phi = n + 1/2$  are identical, hence, periodicity of tunneling conductance takes place with  $\Delta\phi = 1/2$ .
- [70] See Appendix in A.P. Dmitriev, I.V. Gornyi, V.Yu. Kachorovskii, and D.G. Polyakov, arXiv:0911.0911.
- [71] An important modification of results of Ref. [45] in the case of helical ring coupled to magnetic impurity is related to the fact that  $N_R$  and  $N_L$  are non conserved even in the fully closed setup ( $\gamma = 0$ ) because of the impurity-induced backscattering.